

# Disrupted Amygdalar Subregion Functional Connectivity and Evidence of a Compensatory Network in Generalized Anxiety Disorder

Amit Etkin, MD, PhD; Katherine E. Prater, BA; Alan F. Schatzberg, MD; Vinod Menon, PhD; Michael D. Greicius, MD

**Context:** Little is known about the neural abnormalities underlying generalized anxiety disorder (GAD). Studies in other anxiety disorders have implicated the amygdala, but work in GAD has yielded conflicting results. The amygdala is composed of distinct subregions that interact with dissociable brain networks, which have been studied only in experimental animals. A functional connectivity approach at the subregional level may therefore yield novel insights into GAD.

**Objectives:** To determine whether distinct connectivity patterns can be reliably identified for the basolateral (BLA) and centromedial (CMA) subregions of the human amygdala, and to examine subregional connectivity patterns and potential compensatory amygdalar connectivity in GAD.

**Design:** Cross-sectional study.

**Setting:** Academic medical center.

**Participants:** Two cohorts of healthy control subjects (consisting of 17 and 31 subjects) and 16 patients with GAD.

**Main Outcome Measures:** Functional connectivity with cytoarchitecturally determined BLA and CMA regions of interest, measured during functional magnetic reso-

nance imaging performed while subjects were resting quietly in the scanner. Amygdalar gray matter volume was also investigated with voxel-based morphometry.

**Results:** Reproducible subregional differences in large-scale connectivity were identified in both cohorts of healthy controls. The BLA was differentially connected with primary and higher-order sensory and medial prefrontal cortices. The CMA was connected with the midbrain, thalamus, and cerebellum. In GAD patients, BLA and CMA connectivity patterns were significantly less distinct, and increased gray matter volume was noted primarily in the CMA. Across the subregions, GAD patients had increased connectivity with a previously characterized frontoparietal executive control network and decreased connectivity with an insula- and cingulate-based salience network.

**Conclusions:** Our findings provide new insights into the functional neuroanatomy of the human amygdala and converge with connectivity studies in experimental animals. In GAD, we find evidence of an intra-amygdalar abnormality and engagement of a compensatory frontoparietal executive control network, consistent with cognitive theories of GAD.

*Arch Gen Psychiatry.* 2009;66(12):1361-1372

## Author Affiliations:

Department of Psychiatry and Behavioral Sciences (Drs Etkin, Schatzberg, and Menon and Ms Prater), Program in Neuroscience (Drs Menon and Greicius), and Department of Neurology and Neurological Sciences (Dr Greicius), Stanford University School of Medicine, Stanford, California.

**G**ENERALIZED ANXIETY DISORDER (GAD) is a common anxiety disorder in adults, with estimated lifetime prevalence rates of around 5%.<sup>1,2</sup> Generalized anxiety disorder has a long average duration of symptoms<sup>2,3</sup> and is associated with significant quality-of-life impairment or disability.<sup>4</sup> Despite its clinical importance, GAD has received considerably less study than other anxiety disorders. Predictions of which brain circuits are altered in GAD must therefore be extrapolated from findings in other anxiety disorders. A recent meta-analysis from our group<sup>5</sup> showed that post-traumatic stress disorder, social anxiety disorder, and specific phobia—3 of the most frequently studied disorders—are all characterized by hyperactivity of the amygdala and insula of patients during the pro-

cessing of negative emotion. Engagement of the amygdala and insula was also seen in this meta-analysis when healthy subjects experienced fear,<sup>5</sup> suggesting that amygdalar and insular hyperactivation in patients reflects the neural correlates of a current fear or anxiety state or a trait vulnerability for excessive fear responses.

Two recent studies examined amygdala activity in adult patients with GAD in response to viewing fearful faces, a commonly used probe of amygdalar engagement.<sup>6,7</sup> One study found no difference in the amygdala between patients and control subjects,<sup>7</sup> whereas the other study found less activity in the amygdala in patients.<sup>6</sup> By contrast, similar approaches in adolescents with GAD have found hyperactivity in the amygdala.<sup>8,9</sup> Many factors may explain these differences, including differences in baseline amygdalar activity, the ca-

**Table 1. Subject Demographics<sup>a</sup>**

	Study Cohorts			Comparisons
	C1 (n=17)	P (n=16)	C2 (n=31)	
Age, y	32.5 (2.0)	30.6 (1.7)	20.5 (0.2)	C1 > C2 <sup>b</sup> ; C1 vs P, <i>P</i> = .15
Education, y	17.5 (0.5)	17.1 (0.6)	14.3 (0.2)	C1 > C2 <sup>b</sup> ; C1 vs P, <i>P</i> = .34
Female, %	15 (88)	14 (88)	13 (42)	C1 > C2 <sup>c</sup> ; C1 vs P, <i>P</i> > .99
Right-handed, %	17 (100)	16 (100)	31 (100)	<i>P</i> > .99
STAI-T	30.5 (1.3)	56.1 (2.6)	NA	C1 > P <sup>b</sup>
PSWQ	37.1 (2.3)	62.7 (2.3)	NA	C1 > P <sup>b</sup>
BAI	3.8 (1.1)	23.9 (3.2)	NA	C1 > P <sup>b</sup>
BDI-II	2 (0.6)	23.4 (3.3)	NA	C1 > P <sup>b</sup>

Abbreviations: BAI, Beck Anxiety Inventory; BDI-II, Beck Depression Inventory II; C1, generalized anxiety disorder (GAD) control cohort; C2, second control cohort; NA, not acquired; P, GAD patients; PSWQ, Penn State Worry Questionnaire; STAI-T, Spielberger State-Trait Anxiety Inventory.

<sup>a</sup>Unless otherwise indicated, data are expressed as mean (SEM).

<sup>b</sup>*P* < .001.

<sup>c</sup>*P* = .001.

capacity for task-related activation, overall responses to emotional expressions, and the nature and relative levels of GAD psychopathology in each cohort. Nonetheless, these studies leave undefined the role the amygdala plays in GAD. Blair et al<sup>6</sup> used their own data and those of related studies and suggested that an understanding of amygdalar dysfunction in GAD, along with discrepancies between individual studies, will require investigation of the brain network contexts in which the amygdala is involved.

Analyses of functional connectivity using functional magnetic resonance imaging (fMRI) data acquired while the subjects are at rest, unbiased by task demands, have been previously used to identify multiple, simultaneously operating, broadly connected networks of brain regions.<sup>10</sup> Abnormalities in resting functional connectivity have also been identified in major depression.<sup>11</sup> Use of a resting-state approach may therefore provide a useful tool for examining dysfunctional amygdalar-based neural circuitry in GAD.

Our understanding of the organization of the amygdala is derived in large part from investigations of the functions of subnuclei within the amygdala of animals and the distinct brain networks in which they participate. This extensive body of research has established a model wherein sensory information across multiple modalities enters the amygdala through the nuclei of the basolateral complex (BLA) (consisting of lateral, basal, and accessory basal nuclei).<sup>12-16</sup> Neurons in the BLA encode fear memories related to these sensory stimuli, signal the threat value of a stimulus, and can modulate memory encoding and sensory processing in other brain regions.<sup>13,14</sup> The BLA in turn activates the central nucleus, which is essential for the basic species-specific defensive responses associated with fear.<sup>12-16</sup> The central nucleus achieves these functions through projections to brainstem, hypothalamic, and basal forebrain targets.<sup>12-16</sup>

Central to this outlined circuit are anatomical connectivity findings in rodents and nonhuman primates, which differentiate the largely cortical connectivity pattern of the BLA from the largely subcortical connectivity pattern of the central nucleus.<sup>12,15,16</sup> The anatomical connectivity of human amygdalar nuclei, however, is currently unknown. In this study, we therefore examined the differential connectivity patterns of these amygdalar subre-

gions in healthy control subjects and GAD patients to investigate the functional brain networks in which the amygdala is involved and that underlie the distinct functions of these amygdalar subregions.

We first sought to establish whether the functional connectivity of amygdalar subregions can be distinguished in healthy subjects by using resting-state fMRI. Cytoarchitectural, myeloarchitectural, and chemoarchitectural studies of the human amygdala support a differentiation between the BLA and a centromedial subregion (CMA) composed of the central and medial nuclei.<sup>17</sup> We therefore derived regions of interest (ROIs) from cytoarchitecturally determined probabilistic maps of the human BLA and CMA.<sup>18,19</sup> To demonstrate the reliability of this approach, we derived functional connectivity maps from 2 independent control cohorts. We then compared these functional connectivity patterns with those in a matched GAD patient cohort. Finally, we complemented our functional connectivity analyses by performing voxel-based morphometry (VBM), an independent and commonly used structural imaging approach, focusing on gray matter volumes of the BLA and CMA.

## METHODS

### PARTICIPANTS

A total of 64 subjects participated in this study (see **Table 1** for demographics) after giving their informed consent according to institutional guidelines for the protection of human subjects at Stanford University. The first control cohort (GAD controls) and the GAD patients were recruited through local online advertisements. Psychiatric diagnoses based on the *DSM-IV*<sup>20</sup> were determined through an informal clinical interview with a psychiatrist and the structured diagnostic Mini International Neuropsychiatric Interview.<sup>21,22</sup> Exclusion criteria were bipolar, psychotic, or posttraumatic stress disorders or substance abuse diagnoses. Generalized anxiety disorder was the primary diagnosis for all patients. Patients with comorbid major depression were included if the onset of GAD was clearly primary to that of depression. Other exclusion criteria included a history of a neurological disorder, head trauma or loss of consciousness, claustrophobia, and regular use of benzodiazepines, opiates, or thyroid medications. Of the 16 patients, 4 were taking regular antidepressants at a stable dose. No subject used an as-needed dose of a benzodiazepine within 48 hours of the scan. Comorbid

Axis I conditions included major depression (n=4), social anxiety disorder (n=5), panic disorder (n=2), dysthymia (n=2), and obsessive-compulsive disorder (n=1). Of the patients, 6 had no comorbidities, 6 had 1 comorbidity (depression in 3, dysthymia in 2, and social anxiety in 1), and 4 had 2 comorbidities (social anxiety and panic disorder in 2, social anxiety and obsessive-compulsive disorder in 1, and depression and social anxiety in 1). None had more than 2 comorbidities. All GAD controls were free of any current or past Axis I condition and psychiatric medication. No GAD patient had undergone structured psychotherapy. All GAD controls and GAD patients completed the Spielberger State-Trait Anxiety Inventory,<sup>23</sup> the Penn State Worry Questionnaire,<sup>24</sup> the Beck Anxiety Inventory,<sup>25</sup> the Beck Depression Inventory II,<sup>26</sup> and the Mood and Anxiety Symptoms Questionnaire.<sup>27,28</sup> The 31 healthy subjects in the second control cohort were recruited as part of an unrelated study and denied a history of psychiatric or neurological disorders but did not undergo formal evaluation with a structured interview. Data from 22 of these subjects were used previously in an unrelated study.<sup>29</sup>

## fMRI DATA ACQUISITION

All participants underwent an 8-minute resting-state fMRI scan in which they were told to keep their eyes closed, hold still, try not to fall asleep, and allow their minds to wander. Images were acquired on a 3-T scanner (GE Signa scanner; GE Healthcare, Milwaukee, Wisconsin) using a custom-built head coil. A total of 29 axial slices (4.0-mm thickness) covering the whole brain were acquired using a T2-weighted gradient-echo spiral-pulse sequence (repetition time, 2000 milliseconds; echo time, 30 milliseconds; flip angle, 80°; and 1 interleave).<sup>30</sup> The field of view was 22 cm for the GAD controls and GAD patients and 20 cm for the second control cohort, and the matrix size was 64 × 64. To reduce blurring and signal loss arising from field inhomogeneities, an automated high-order shimming method based on spiral acquisitions was used before acquiring fMRI scans.<sup>31</sup> A high-resolution T1-weighted spoiled grass gradient-recalled inverted recovery 3-dimensional MRI sequence was used with the following parameters: time after inversion pulse, 300 milliseconds; repetition time, 8 milliseconds; echo time, 3.6 milliseconds; flip angle, 15°; field of view, 22 cm; 124 slices in the coronal plane; 256 × 192 matrix; number of excitations, 2; and acquired resolution, 1.5 × 0.9 × 1.1 mm. The images were reconstructed as a 124 × 256 × 256 matrix with a 1.5 × 0.9 × 0.9-mm spatial resolution. Structural and functional images were acquired in the same scan session.

## fMRI DATA ANALYSIS

### Preprocessing

The first 8 volumes were not analyzed to allow for signal equilibration effects. A linear shim correction was applied separately for each slice during reconstruction using a magnetic field map acquired automatically by the pulse sequence at the beginning of the scan.<sup>30</sup> The fMRI data were then preprocessed using SPM5 software (available at: <http://www.fil.ion.ucl.ac.uk/spm/>) implemented in a MATLAB suite (Mathworks, Inc, Natick, Massachusetts). Images were realigned to correct for motion, corrected for errors in slice timing, spatially transformed to standard stereotaxic space (based on the Montreal Neurologic Institute coordinate system),<sup>32</sup> resampled every 2 mm, and smoothed with a 6-mm full-width half-maximum gaussian kernel. There were no participants with movement greater than 3 mm of translation or 3° of rotation. There were also no significant differences between the total range of movement across any axis of translation or rotation between groups. Data were then bandpass filtered using FMRIB Software Library tools (available at: <http://www.fmrib.ox>

.ac.uk/fsl/index.html) to retain frequencies from 0.008 to 0.1 Hz, to remove high- and low-frequency noise sources, and to allow for better discrimination of low-frequency resting-state networks. Most of the power in resting-state networks is found in this low-frequency band.<sup>33</sup>

### Functional Connectivity Analyses

Seeds for the connectivity analysis corresponded to the BLA and CMA subregions<sup>34</sup> and were constructed from maximum probability maps of these 2 subregions, defined through the Anatomy Toolbox in SPM5.<sup>19</sup> Maximum probability maps allow the definition of nonoverlapping regions from underlying probability maps that are inherently overlapping.<sup>18,19</sup> Voxels were included in the maximum probability maps if the probability of their being assigned to the BLA or CMA was higher than for other nearby structures, such as other amygdalar subregions or medial temporal lobe structures, with no less than 40% likelihood.<sup>19</sup> The BLA and CMA maximum probability maps were then converted to ROIs using a toolbox for SPM (MarsBaR [MARSeille Boite À Région d'Intérêt]; available at <http://marsbar.sourceforge.net/>), and the individual time series within each ROI was obtained from bandpass-filtered images. Each time series was then put into a first-level fixed-effects general linear model in SPM5,<sup>35</sup> and 4 separate connectivity analyses were then performed for each subject (2 ROIs per side). A global signal regressor and the 6 motion parameters for each subject were included as covariates of no interest in each model. For direct correlations of ROI time courses, variance associated with the global mean or motion parameters was removed before performing the correlations. A similar approach was taken in a control connectivity analysis in which the primary auditory cortex was the seed region, using a previously defined ROI.<sup>36</sup>

### Group-Level Analyses

We performed group-level analyses using the contrast images from the individual functional connectivity analyses in random-effects *t* tests or analyses of variance (ANOVAs). The ANOVAs were performed with a flexible factorial model in which a subject factor was additionally used to model the sphericity of the data appropriately. All group-level analyses were masked with a map from 1-sample *t* tests of each relevant group, thresholded leniently at  $P = .05$ , uncorrected, and then combined across side and region to restrict connectivity analyses to positively correlated voxels only. This procedure avoided potential interpretational confounds related to apparently negative connectivity resulting from correction for global signal changes.<sup>37</sup> Statistical thresholds were set at  $q < 0.05$ , whole-brain corrected for the false discovery rate. Connectivity foci were labeled by comparison with neuroanatomical atlases.<sup>38</sup> Reported voxel coordinates correspond to standardized Montreal Neurologic Institute space. Because the BLA cortical targets formed 1 very large cluster at  $q < 0.05$ , whole-brain corrected, we report representative differential connectivity peaks separately for each lobe in **Table 2** and limit the number of peaks to no more than 3 per region for clarity of presentation. For the displayed sections, the right side of the image corresponds to the right side of the brain.

To determine the connectivity specificity of amygdalar subregions with their respective targets, average connectivity ( $\beta$  weights) in volumes of interest were extracted from CMA- or BLA-seeded connectivity analyses (separated by side) using masks generated from the ANOVA effect of region for the GAD control cohort (separately for BLA or CMA targets). The volume of interest data then underwent ANOVA using commercially available statistical software (SPSS; SPSS Inc, Chicago, Illinois). Identical masks were used for both control cohorts and the GAD patient group. All error bars or standard error ranges reported refer to standard errors of the mean.

**Table 2. Conjunction Analysis Connectivity Peaks**

Region <sup>a</sup>	Peak	Side	Voxel Coordinates <sup>b</sup>			z Score	
			x	y	z		
BLA > CMA <sup>c</sup>							
Frontal lobe	Precentral gyrus	R	38	-28	62	6.34	
	Precentral gyrus	R	46	-18	50	5.11	
	Precentral gyrus	L	-58	-18	38	4.53	
	Orbitofrontal cortex	L	-36	38	-18	4.18	
	Orbitofrontal cortex	R	36	28	-20	3.83	
	Ventromedial PFC	L	-4	54	-16	4.13	
Parietal lobe	Inferior/middle frontal gyrus	L	-44	16	20	3.43	
	Postcentral gyrus	R	38	-30	64	6.39	
	Postcentral gyrus	R	46	-22	52	5.28	
	Postcentral gyrus	L	-54	-22	48	4.51	
	Superior parietal lobule	R	22	-84	34	4.63	
	Superior parietal lobule	L	-20	-80	34	4.58	
Occipital lobe	Intraparietal sulcus	R	28	-60	58	3.76	
	Intraparietal sulcus	L	-24	-56	58	3.48	
	Inferior/middle occipital gyrus	R	42	-80	6	5.89	
	Inferior/middle occipital gyrus	L	-48	-74	4	4.91	
	Fusiform gyrus	R	26	-66	-8	5.36	
	Fusiform gyrus	L	-16	-82	-8	4.58	
	Fusiform gyrus	R	30	-86	-8	4.41	
	Lingual gyrus	L	-22	-52	-4	5.18	
	Middle/superior occipital gyrus	R	22	-88	30	4.96	
	Middle/superior occipital gyrus	L	-16	-88	24	4.88	
Temporal lobe	Occipital pole	R	8	-90	18	4.56	
	Superior temporal sulcus/gyrus	R	54	-2	-12	5.56	
	Superior temporal sulcus/gyrus	L	-62	-16	2	4.83	
	Parahippocampal gyrus	L	-22	-50	-6	5.46	
	Parahippocampal gyrus	R	24	-50	-2	5.06	
	Temporal pole	L	-40	12	-32	5.23	
	Temporal pole	R	36	10	-32	4.53	
	Middle temporal gyrus	R	44	-60	2	5.13	
	Middle temporal gyrus	L	-54	-6	-26	4.58	
	Fusiform gyrus	R	34	-34	-20	4.26	
	Inferior temporal gyrus	R	46	-58	-18	4.48	
	Inferior temporal gyrus	L	-44	-54	-18	4.08	
CMA > BLA <sup>d</sup>							
Thalamus/caudate/amygdala	Superior temporal gyrus/planum temporale	R	62	-40	10	4.46	
	Superior temporal gyrus/planum temporale	L	-44	-36	12	4.21	
	Pulvinar/caudate (body)	L	-18	-22	18	6.63	
	Pulvinar/caudate (body)	R	22	-26	16	6.16	
	Septal nuclei/fornix	L/R	-2	4	18	5.51	
	Centromedial amygdala	L	-26	-14	-4	5.38	
	Caudate (body)	R	18	-4	26	5.38	
	Midline thalamus	L/R	-2	-14	10	5.25	
	Midline thalamus	L/R	2	-6	8	5.12	
	Lateral thalamus	R	20	-12	10	5.12	
	Septal nuclei/fornix	L/R	-4	-18	24	4.96	
	Centromedial amygdala	R	26	-16	-4	4.65	
	Anterior thalamus (reticular nucleus, BNST)	L/R	10	-4	6	4.42	
	Pulvinar	L	-8	-28	12	4.39	
VTA/SN/PAG	VTA/SN	L/R	6	-20	-16	4.26	
	PAG	L/R	-4	-28	-12	3.51	
	Cerebellum	Vermis	L/R	-2	-56	-32	4.11
	Cerebellum	Posterior	L/R	-4	-80	-26	4.08
	Cerebellum	Lateral	L	-26	-62	-28	3.98
	Insula	...	R	38	10	12	3.48
	Cerebellum	Lateral	R	34	-54	-32	3.46
	Cerebellum	Lateral	R	30	-70	-26	3.38

Abbreviations: BLA, basolateral amygdalar subregion; BNST, bed nucleus of the stria terminalis; CMA, centromedial amygdalar subregion; ellipses, not applicable; L, left side; PAG, periaqueductal gray; PFC, prefrontal cortex; R, right side; SN, substantia nigra; VTA, ventral tegmental area.

<sup>a</sup>Described as large, contiguous cortical cluster divided by lobe.

<sup>b</sup>Based on the Montreal Neurologic Institute coordinate system.

<sup>c</sup>Indicates BLA connectivity is increased compared with CMA connectivity.

<sup>d</sup>Indicates CMA connectivity is increased compared with BLA connectivity.

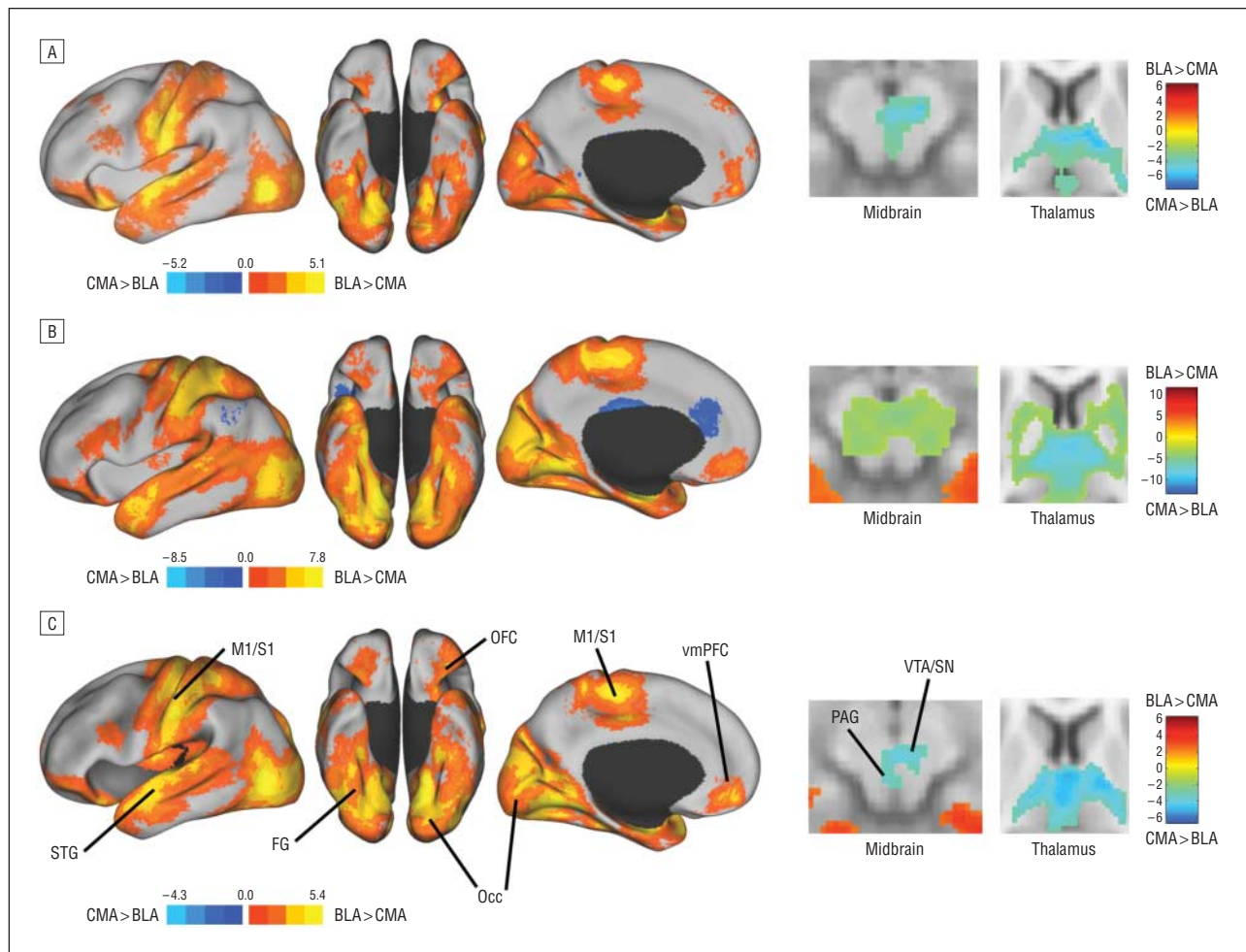


**Figure 1.** Differential connectivity of the basolateral (BLA) and centromedial (CMA) amygdalar subregions during resting-state functional magnetic resonance imaging. Findings are shown in 2 separate cohorts of healthy subjects (A and B) and a formal conjunction between these cohorts (C). The BLA connectivity was primarily cortical, whereas the CMA connectivity was primarily subcortical. Color scales represent *t* scores for the main effect of region in a voxelwise analysis of variance. Red indicates that BLA connectivity is increased compared with CMA connectivity; blue, CMA connectivity is increased compared with BLA connectivity. FG indicates fusiform gyrus; M1/S1, primary somatosensory and motor cortices; Occ, occipital cortex; OFC, orbitofrontal cortex; PAG, periaqueductal gray; STG, superior temporal gyrus; vmPFC, ventromedial prefrontal cortex; and VTA/SN, ventral tegmental area/substantia nigra.

## STRUCTURAL DATA ANALYSIS

Voxel based morphometry was performed using the VBM5 toolbox in SPM5 (Wellcome Department of Cognitive Neurology, London, England; available at: <http://dbm.neuro.uni-jena.de/vbm/vbm5-for-spm5/>). The individual T1-weighted images from the GAD controls and the matched GAD patient group were segmented using a unified segmentation routine through the VBM5 toolbox.<sup>39</sup> The segmented, modulated gray matter images were then smoothed at 6 mm full width half maximum.<sup>40</sup> The volumes of interest corresponding to gray matter volume (modulated images) were extracted for the BLA and CMA on both sides for statistical analyses in SPSS.

## RESULTS

### DISSOCIABLE AND REPRODUCIBLE CONNECTIVITY NETWORKS FOR BLA AND CMA

We initially examined a cohort of 17 well-characterized healthy subjects (the GAD controls) (Table 1) by conducting resting-state fMRI connectivity analyses separately for

each of the 2 amygdalar subregion ROIs across both sides of the brain while controlling for variations in global signal (described in the “Functional Connectivity Analyses” subsection of the “Methods” section). In this cohort, the BLA and CMA ROIs explained 21% of the variance in the other ROI during our resting-state fMRI scans, suggesting that these ROIs have enough nonshared variance to allow for identification of differential connectivity patterns.

Next, we performed a set of connectivity analyses, using the BLA and CMA ROIs as seeds, which we entered into a voxelwise ANOVA. Directly contrasting BLA and CMA connectivity (collapsing across sides) yielded robust, spatially coherent patterns of differential connectivity (**Figure 1** A). The connectivity patterns were bilateral and similar for ROIs from the right and left sides (data not shown), and there were no significant connectivity clusters in the region  $\times$  side ANOVA interaction analysis ( $q < 0.05$ ; data not shown).

The BLA was associated with exclusively cortical differential connectivity, encompassing bilaterally the entire occipital lobe, large extents of the ventral temporal lobe,

superior temporal gyrus and sulcus, precentral and postcentral gyri, intraparietal sulcus, lateral posterior orbitofrontal cortex, dorsal and ventral medial prefrontal cortex (PFC), parahippocampal gyri, and a small region in the inferior lateral PFC (Figure 1A). This broad neural network includes primary and higher-order association cortices for the visual, somatosensory, and auditory systems, as well as motor regions, areas important in memory formation, and higher-order areas in the PFC, most notably along its medial and inferior aspects. The CMA was associated almost exclusively with subcortical differential connectivity, including the thalamus (in particular along the midline), midbrain (in the region of the substantia nigra, ventral tegmental area, and periaqueductal gray), medulla, cerebellum (in particular in the vermis), and caudate (Figure 1A).

To determine the robustness and replicability of these connectivity patterns, we examined a second, unrelated group of 31 healthy adults (second control cohort) and replicated the differential connectivity patterns for the BLA and CMA that had been identified in the GAD controls (Figure 1B). The only difference in connectivity results between these cohorts consisted of insular, dorsal anterior cingulate, and midcingulate CMA connectivity in the second control cohort. To directly and quantitatively identify those regions with the most robust and reproducible pattern of differential BLA and CMA connectivity, we conducted a formal conjunction analysis across the 2 independent control cohorts (Figure 1C and Table 2).<sup>41</sup> This analysis confirmed the exclusively cortical pattern of differential BLA connectivity and the subcortical pattern of differential CMA connectivity, as detailed in the preceding paragraphs.

To further quantify the differential connectivity patterns, we constructed a separate mask for BLA and CMA targets derived only from the GAD controls, removing amygdalar voxels to avoid the potentially confounding effects of correlations of ROIs with themselves. We determined the average connectivity of the BLA or CMA target networks with the BLA and CMA source ROIs from both sides (Figure 2A). As expected, in the GAD control cohort, we found a strong reciprocal difference in BLA and CMA connectivity with their respective targets (eg, stronger connectivity of BLA ROIs with BLA targets than CMA targets; ANOVA region  $\times$  target interaction,  $P < .001$ ), which was consistent across both sides (ANOVA side  $\times$  region  $\times$  target interaction,  $P = .38$ ). Strikingly, we found highly similar results for the second control cohort, using the target network defined only from the GAD controls (ANOVA region  $\times$  target interaction,  $P < .001$ ; region  $\times$  side  $\times$  target interaction,  $P = .59$ ). The 2 control cohorts, moreover, did not differ in their pattern of differential BLA-CMA connectivity (ANOVA group  $\times$  region  $\times$  target interaction,  $P = .63$ ). This dissociable pattern of amygdalar subregional connectivity in the second control cohort was captured by target networks independently defined from the ANOVA on just the GAD controls. Performing the analysis in this way would, if anything, be expected to reduce our sensitivity for finding subregional connectivity differences in the second control cohort and thus speaks to the robustness of these findings.

Finally, we examined the relationship between target region connectivity and cytoarchitectonic probability of

individual amygdalar voxels by performing seeded connectivity analyses for both control cohorts using the entire BLA or the CMA target network, defined from just the GAD controls, as source ROIs. We then extracted the connectivity strength and cytoarchitectonic probability for each voxel in the amygdala. The probability of belonging to the BLA or CMA was found to significantly and positively predict that voxel's connectivity with the BLA or CMA target network, respectively, on both the right and left sides for the GAD controls ( $P < .001$  for all comparisons). This relationship also held true for the second control cohort, despite the fact that the target networks were derived from the ANOVA data of the GAD controls ( $P < .001$  for all comparisons).

#### AMYGDALAR SUBREGIONAL CONNECTIVITY AND ANATOMY IN GAD

We next wanted to determine whether an amygdalar subregional connectivity analysis could provide insight into GAD. In 16 GAD patients who were age-, sex-, and education-matched to the GAD controls (see Table 1), we examined the connectivity strength of the BLA and CMA ROIs with the target networks identified from the GAD controls (Figure 2A). Whereas the 2 independent control cohorts showed similarly robust differential subregional connectivity, the GAD patients showed less distinct subregion-target connectivity patterns (ANOVA group  $\times$  region  $\times$  target interaction,  $P = .003$ ; partial  $\eta^2 = 0.25$ ), although these patients still showed some degree of dissociation between BLA and CMA target connectivity (ANOVA region  $\times$  target interaction for GAD patients only,  $P = .001$ ). This group difference in specificity of subregional connectivity was driven by decreased connectivity in patients between the BLA or CMA and their respective targets and by increased connectivity with the other subregion's targets (Figure 2A). This effect can also be clearly seen in Figure 3A and B, in which the ANOVA effects of group are shown separately for each subregion. In Figure 3A, decreased connectivity of the GAD patients' BLA with BLA targets is shown in blue (eg, occipitotemporal cortex, superior temporal gyrus, somatomotor cortices, and medial PFC). Similarly, increased connectivity of GAD patients' CMA with the same BLA targets is shown in red in Figure 3B. This voxelwise analysis also revealed greater BLA connectivity in GAD patients with normal CMA targets (the thalamus, brainstem, and cerebellum) and decreased CMA connectivity with its normal targets (data not shown). Thus, the target network approach in Figure 2A, in which amygdalar connectivity with all significant voxels was averaged into a single summary value, yielded the same results as the voxelwise analysis and thereby provided a simple graphic representation of the findings. Moreover, the group  $\times$  region  $\times$  target interaction finding remained significant after controlling for the regular use of psychiatric medication ( $P = .01$ , partial  $\eta^2 = 0.19$ ) or the presence of comorbid major depressive disorder ( $P = .008$ , partial  $\eta^2 = 0.21$ ), a psychiatric condition closely related to GAD. Furthermore, comparisons of subgroups based on the use of psychiatric medication or the presence of comorbid depression did not yield significant differences.

We next examined whether the group differences in amygdalar connectivity reflected a global alteration of rest-

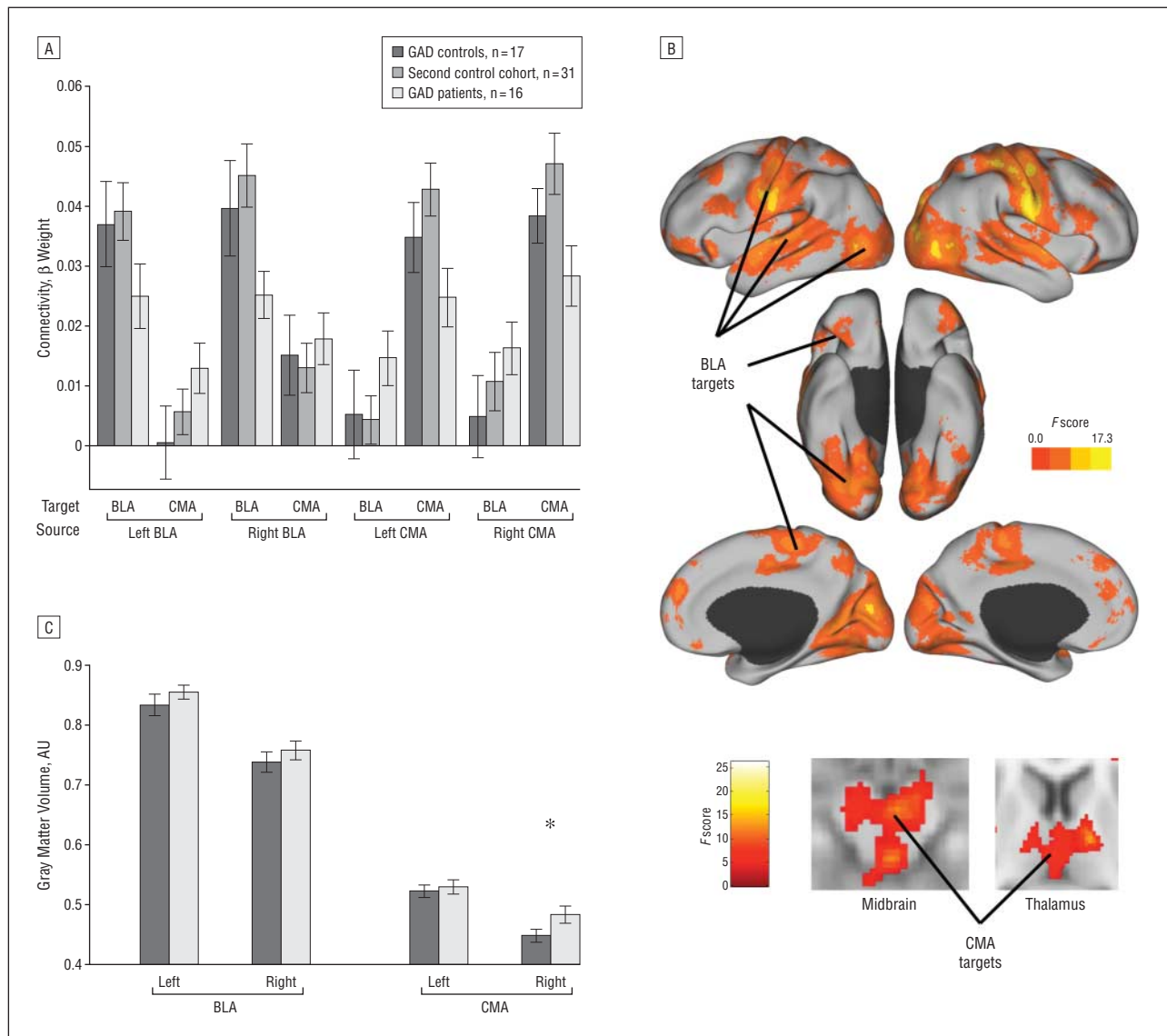


**Figure 2.** Specificity of amygdalar subregion connectivity with target regions in healthy subjects and patients with generalized anxiety disorder (GAD). **A**, Connectivity of the basolateral (BLA) or the centromedial (CMA) amygdalar regions of interest (ROIs), separately on the right and left sides, with target networks defined by differential BLA vs CMA connectivity maps from the analysis of variance (ANOVA) effect of region analysis from just the first control cohort (GAD controls) (shown in Figure 1A). Dissociable patterns of BLA and CMA connectivity (eg, greater connectivity of BLA ROIs with BLA targets than with CMA targets, and the reverse for CMA ROIs) were found to a similar degree in both control cohorts but were significantly reduced in GAD patients, who were demographically matched with the GAD controls. Bars represent mean values; error bars, standard error of the mean. **B**, Results of a voxelwise group  $\times$  region ANOVA comparing differential BLA-CMA connectivity in healthy controls and GAD patients. Significance in this analysis would mean that there is a group difference in the dissociability of BLA-CMA connectivity because of decreased connectivity with the correct targets or because of increased connectivity with the incorrect targets in 1 group. That BLA and CMA targets (see labels) are significant suggests that there is an intra-amygdalar subregional disorganization in the GAD patients rather than alterations in the connectivity of the amygdala with some targets but not others. Results are displayed at  $P = .05$ , uncorrected, to ensure a complete view of group differences. The color scales reflect  $F$  scores from the ANOVA. **C**, A voxel-based morphometry analysis of structural magnetic resonance images from the GAD controls and GAD patients, focusing on the amygdalar subregions used for the functional connectivity analyses, identified increased gray matter volume in the right CMA subregion in GAD patients.  $*P = .03$ . Bars represent mean values; error bars, standard error of the mean. AU indicates arbitrary units.

ing-state connectivity in patients, by examining connectivity within a control network previously reported by our group.<sup>36</sup> We found that the primary auditory cortex was strongly connected to its contralateral homologue in both control cohorts (left seed target peak voxel coordinates, 54, -18, 8 [ $z = 6.0$ ]; right seed, -46, -25, 4 [ $z = 4.87$ ]) and patients (left seed, 46, -16, 8 [ $z = 6.03$ ]; right seed, -52, -16, 6 [ $z = 5.51$ ]), with no difference between groups at  $q < 0.05$ . The amygdalar connectivity findings are therefore not due to global changes in resting-state connectivity.

Differences in subregional connectivity in patients using the whole-network masks may be due to an intra-amygdalar alteration (eg, in subregional size, shape, or cellular composition) or a change in the connectivity of the amygdala with specific target brain regions. To distinguish between these 2 possibilities, we performed a voxelwise ANOVA group  $\times$  region analysis and displayed it at a lenient threshold to avoid false-negative results. Significance in this analysis would mean that there is a group difference in the dissociability of BLA-CMA connectivity, because of decreased connectivity with the correct targets or

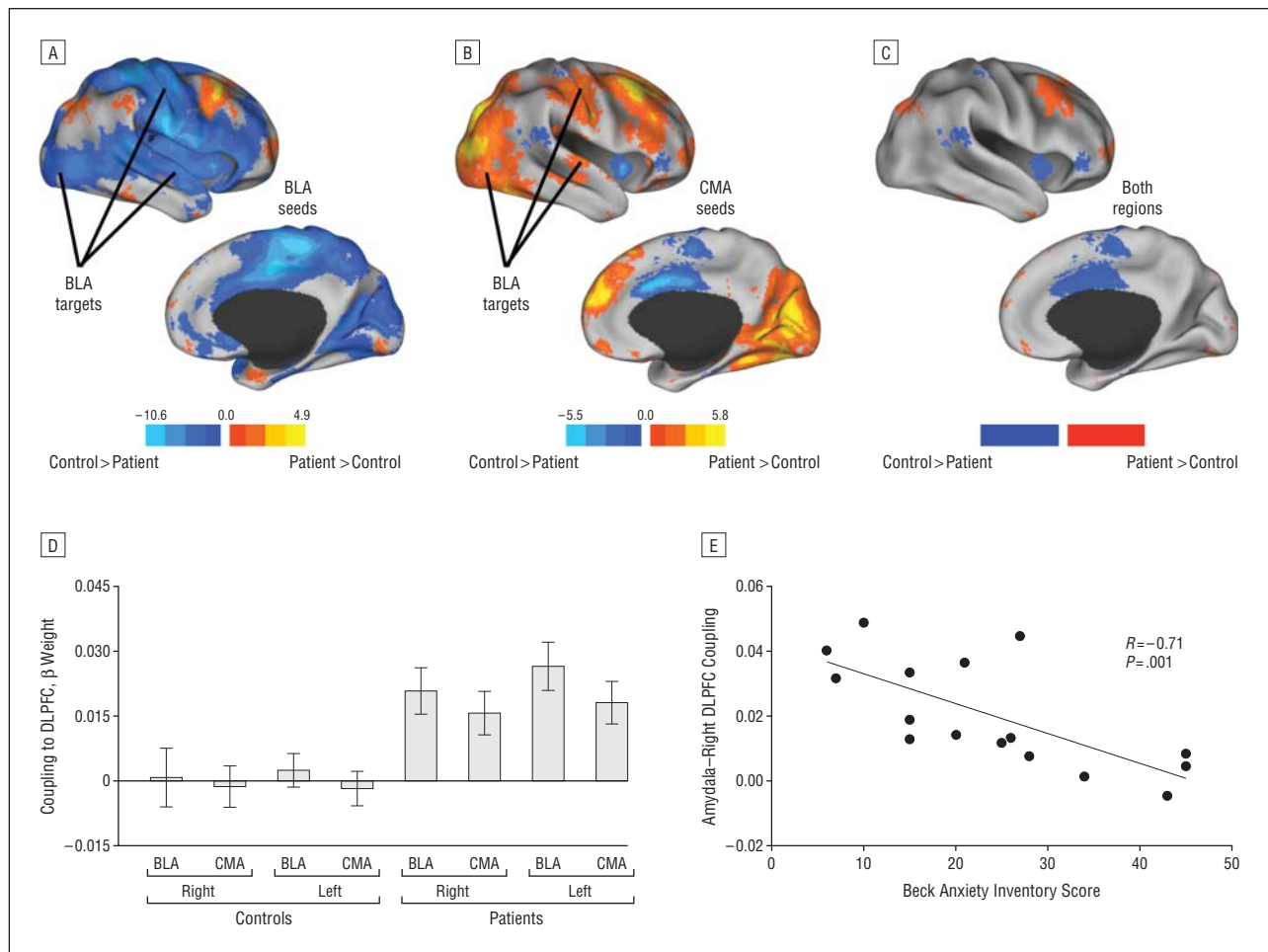


**Figure 3.** Group connectivity differences across amygdalar subregions and evidence of a compensatory network in generalized anxiety disorder (GAD). A, The analysis of variance (ANOVA) effect of group is shown for the basolateral amygdalar subregions (BLA). B, The ANOVA effect of group is shown for the centromedial amygdalar subregions (CMA). Red indicates connectivity was increased in GAD patients compared with control cohorts; blue, connectivity was increased in control cohorts compared with GAD patients. Thus, the majority of blue in part A indicates decreased connectivity of GAD patients' BLA to normal BLA targets, whereas the majority of red in part B indicates increased inappropriate connectivity of GAD patients' CMA to normal BLA targets. C, Common increased or decreased connectivity in GAD patients across both amygdalar subregions identifies a bilateral frontoparietal network with increased connectivity (red) and a bilateral insulocingulate network with decreased connectivity (blue). For figure clarity, only the right side of the brain is shown. D, Subregional connectivity of the right dorsolateral prefrontal cortex (DLPFC) from part C in controls and GAD patients demonstrates that this is an adaptation in patients not normally seen in controls. Bars represent mean values; error bars, standard error of the mean. E, Average connectivity of the right DLPFC to the amygdala in GAD patients is negatively correlated with anxiety scores, suggesting that it reflects connectivity with a compensatory network.

increased connectivity with the incorrect targets in 1 group. We found similar ANOVA significance diffusely across all BLA or CMA target regions (Figure 2B). These data argue, therefore, that there is an intra-amygdalar perturbation in subregional organization in GAD rather than an alteration in the connectivity of the amygdala selectively with some targets but not others. In additional support of this idea, we found that time courses from the BLA and CMA ROIs were more highly correlated in the GAD patients than in the control cohorts ( $P = .002$ , Cohen's  $d = 1.2$ ), accounting for nearly twice as much of each others' variance as in the controls (37% vs 21%), thus consistent with GAD patients having less distinct subregional connectivity patterns.

To further test the idea that amygdalar structure is altered at the subregional level in GAD, we sought convergent evidence from a complementary neuroimaging modality sensitive to changes in brain structure. To do so, we conducted a VBM analysis of gray matter volume within the amygdala, using the same maximum probability maps

as for the functional connectivity analysis because this was the greatest level of neuroanatomical detail for which we sought to make conclusions. We found a significant increase in gray matter volume in GAD patients (modulated images; ANOVA effect of group,  $P = .01$ , partial  $\eta^2 = 0.55$ ), which was most notable within the right CMA (Figure 3C; 2-sample  $t$  test,  $P = .03$ ; Cohen's  $d = 0.78$ ). These data therefore provide convergent evidence for an intra-amygdalar perturbation at the level of individual subregions in GAD patients, using an independent measure of brain structure from anatomical (nonfunctional) brain scans.

In examining the group differences in BLA or CMA connectivity (Figure 3A and B), we also found that several regions consistently showed increased or decreased connectivity in patients using seeds in either of the 2 subregions—an effect orthogonal with the decreased subregional specificity of connectivity that we have already noted in patients. To explore these findings, we identified those voxels in which GAD patients had increased (red) or decreased (blue) con-

nectivity with both amygdalar subregions (Figure 3C). We were particularly intrigued by the finding of increased dorsolateral PFC (DLPFC)–amygdalar connectivity in the GAD patients because we did not find amygdalar connectivity with this region or the posterior parietal cortex in our control cohorts. Indeed, extraction of data for the DLPFC revealed no connectivity with either subregion in the controls but consistently increased connectivity with both subregions in the GAD patients (Figure 3D). Moreover, average DLPFC–amygdalar connectivity in the GAD patients was negatively correlated with all anxiety measures, most notably with the Beck Anxiety Inventory (Figure 3E). These data therefore suggest that a lateral prefrontal executive control network is abnormally coupled with the amygdala in GAD patients. That this connectivity is strongest in the least anxious patients strongly suggests a compensatory neural adaptation.

## COMMENT

To study amygdalar subregional connectivity in GAD, we first investigated whether the functional connectivity patterns of the BLA and CMA can be robustly discriminated using resting-state fMRI in healthy controls and whether these abide by predictions of anatomical connectivity derived from experimental animals. As with these anatomical studies, our study focused on differential connectivity, thus being sensitive to subregional differences in connectivity even if there is some anatomical connectivity of the BLA and CMA with the same targets. Anatomical tract tracing studies in nonhuman primates have determined that a wide range of cortical regions, primarily with sensory functions or in the medial PFC, provide input preferentially into the BLA and frequently receive reciprocal projections from the BLA.<sup>12,16</sup> Studies in rodents have generally supported this view,<sup>15</sup> although some discrepancies exist across species. We found robust and highly reproducible differential connectivity between the BLA and the entire occipital lobe and large parts of the temporal lobe. These targets represent primary and higher-order association cortices for the visual and auditory systems, with likely equal sensitivity to afferent and efferent connections. We also found strong differential connectivity of the BLA to the ventromedial PFC, posterior orbitofrontal cortex, and parahippocampal gyrus. In nonhuman primates, the medial and orbital PFC and the entire temporal lobe are primarily connected with the BLA, although portions of these regions also have light connectivity with the central or medial nuclei.<sup>42,43</sup> Our data are therefore consistent with predictions from connectivity studies in experimental animals.

By contrast with animal connectivity studies, we found robust and highly reproducible differential BLA connectivity bilaterally with the primary motor and primary somatosensory cortices throughout their mediolateral course. In nonhuman primates, no evidence supports amygdalar connectivity with either region,<sup>44,45</sup> although in rodents limited evidence supports amygdalar connectivity with both regions.<sup>46</sup> Additional work will be necessary to determine whether these findings reflect species-specific differences in amygdalar connectivity, greater sensitivity of our functional connectivity method compared with ana-

tomical connectivity methods, or connectivity of the amygdala and sensory/motor cortex via a third region.

Finally, anatomical studies in nonhuman primates have generally reported absent or very sparse connectivity of the amygdala with lateral PFC, with connectivity most notable within the posterior inferior frontal gyrus.<sup>47,48</sup> Within the lateral PFC, we found differential BLA connectivity most robustly also in the posterior inferior frontal gyrus. The connectivity of the BLA with this region of the lateral PFC, as well as with the ventromedial PFC, thus provides evidence of a tight relationship among these 3 regions—a relationship that is thought to be important for emotion regulation through cognitive control.<sup>49–52</sup>

The CMA is composed of the central and medial nuclei, which are thought to constitute a closely related functional subsystem within the amygdala.<sup>17</sup> In humans, the central nucleus represents most of the volume of the CMA,<sup>38</sup> and thus we focus primarily on its connectivity and functions, in particular in light of a role of the central nucleus in the expression of fear, regulation of arousal, and patterning of behavior<sup>13,14</sup> and the overall similar connectivity of these 2 nuclei.<sup>12,15,53</sup> Input into the central nucleus comes from a range of subcortical regions, including midline thalamic and anterior gustatory nuclei, hypothalamus, midbrain and pontine reticular formations, and viscerosensory and neuromodulatory brainstem nuclei.<sup>12,15,53</sup> The central nucleus projects to many of the regions from which it receives input, as well as to the pulvinar,<sup>12,15,16,53</sup> the mediodorsal thalamic nucleus,<sup>54</sup> and the effector nuclei in the brainstem.<sup>12,15,16</sup>

Consistent with this pattern of anatomical connectivity in rodents and nonhuman primates, we found prominent differential CMA connectivity across most of the thalamus (most notably along the midline) and in the pulvinar. Activation of the midline thalamic nuclei is seen during endogenous and learned fear in rodents<sup>55,56</sup> and is associated with viscerosensory functions.<sup>57</sup> Finally, we found differential CMA connectivity with a midbrain region containing the ventral tegmental area and substantia nigra and extending posteriorly to the periaqueductal gray. Our findings of functional connectivity of the CMA with these regions are, therefore, consistent with findings of anatomical studies in animals.<sup>12,15,16</sup>

Strong differential connectivity of the CMA was also seen with the cerebellum, most notably with the vermis—connectivity that is not generally discussed in animal tract-tracing studies. The vermis has been implicated in endogenous and learned fear,<sup>58–60</sup> and vermis stimulation leads to amygdalar synaptic potentials with latencies consistent with monosynaptic connections.<sup>61,62</sup> Our results, therefore, strengthen evidence of a role of the cerebellum—and in particular the vermis—in emotional processes<sup>63</sup> through connectivity with the CMA.

Generalized anxiety disorder has received less intense neurobiological study than other anxiety disorders, in which amygdalar hyperactivity in patients during the processing of negative emotion has been a consistent finding.<sup>5</sup> The issue of whether amygdalar abnormalities exist in adults with GAD has been unresolved, in part because the amygdala's context within distributed brain networks appears to be important<sup>6</sup> but has not previously been a focus of investigation. In this study, we found evidence of an intra-

amygdalar perturbation in GAD and abnormal connectivity of the amygdala with at least 2 distinct brain networks.

By first focusing on differential amygdalar subregional connectivity patterns, we found that, although GAD patients still showed evidence of differential BLA-CMA connectivity, this difference was considerably less robust than in controls. Further investigation revealed that this finding was due to disorganization at an intra-amygdalar subregional level in the GAD patients. This conclusion is supported by (1) a higher correlation between BLA and CMA time series in the GAD patients than in the controls, (2) the lower connectivity of the BLA or the CMA of GAD patients to all of their normal targets and increased connectivity to all of the other subregions' targets, and (3) our finding of increased amygdalar gray matter volume in GAD patients (in particular within the right CMA) using a VBM approach with structural scans acquired from the same subjects. These findings therefore provide evidence that GAD, like other anxiety disorders, involves important alterations in the amygdala, even if these have not been consistently detected during emotional activation paradigms. Moreover, our data raise new questions about how to interpret hypoactivation or the absence of differences in amygdalar activation in GAD in light of subregional disorganization within the amygdala.

Another striking finding in GAD patients was the presence of significantly increased or decreased connectivity of several regions with both amygdalar subregions. We found significant decreased amygdalar connectivity bilaterally with the insula, dorsal/midcingulate, supplementary motor area, thalamus, caudate, putamen, superior temporal gyrus, and ventrolateral PFC. Extraction of data from the insula and cingulate revealed that, in controls, these regions were connected with both amygdalar subregions (data not shown). This connectivity pattern closely resembled a previously identified resting-state network, implicated in salience processing, which consists of limbic and paralimbic regions and of which the amygdala is normally a part.<sup>64</sup> Activation in these regions, most notably in the fronto-insular and dorsal anterior cingulate cortices, tends to track with sympathetic nervous system arousal.<sup>65</sup> Aberrant autonomic nervous system activity has been noted in GAD, and in particular a decrease in autonomic flexibility,<sup>66,67</sup> suggesting that decreased coupling of the amygdala to the salience network may be related to abnormalities in modulation of the autonomic nervous system. Further work, however, will be needed to explore this possibility, which at present remains speculative.

Significantly increased amygdalar connectivity was seen bilaterally with the dorsolateral, ventrolateral, dorsomedial, and ventromedial PFCs; posterior parietal cortices; and inferior occipitotemporal cortices. This pattern closely resembles the canonical frontoparietal executive control network identified in many studies of cognitive control over emotional<sup>49</sup> and nonemotional<sup>68,69</sup> material. This coordinated network has also been observed using resting-state fMRI and has been reliably dissociated from the salience network.<sup>64</sup>

At rest, the executive control network in healthy controls does not normally include the amygdala,<sup>64</sup> and thus coupling of the amygdala with this network in patients likely reflects a network-level neural adaptation in GAD. Extrac-

tion of data from the DLPFC and posterior parietal cortices bilaterally confirmed that none of these regions was connected with either amygdalar subregion in controls (Figure 3; other data not shown). Amygdalofrontoparietal coupling in GAD patients may thus reflect the habitual engagement of a cognitive control system to regulate excessive anxiety. Indeed, cognitive theories of GAD suggest that the use of compensatory cognitive strategies, such as worry, reflects attempts at diminishing the impact of emotions, with which GAD patients are otherwise less able to deal.<sup>70,71</sup> The negative correlation between amygdala-DLPFC coupling and anxiety furthermore suggests a relationship between this adaptation and successful control of anxiety.

Aberrant coupling of the BLA and CMA with the DLPFC is also consistent with several other recent findings. Greater right DLPFC activation has been found in GAD patients during emotional processing.<sup>6</sup> A magnetic resonance spectroscopy study focusing on the DLPFC found a higher *N*-acetylaspartate to creatinine ratio, a marker of neuronal viability, in GAD patients.<sup>72</sup> Moreover, the right DLPFC has recently been successfully targeted in a small open-label treatment study of GAD using transcranial magnetic stimulation.<sup>73</sup> In sum, our findings demonstrate abnormal engagement of the amygdala in at least 2 distinct brain networks and argue that one of these networks reflects a compensatory neural adaptation, consistent with cognitive theories of GAD.

Several limitations are also important to mention. We used conventional fMRI methods in this study, and, as such, one concern may be that the limited spatial resolution of conventional fMRI may be insufficient for discriminating between amygdalar subregions. We and others<sup>74-76</sup> have used activation task-based approaches to demonstrate that amygdalar subregions may be functionally differentiated during emotional processing. In the present study, despite the use of conventional fMRI acquisition parameters, the BLA and CMA were associated with dramatically different connectivity patterns, which were highly replicable and consistent with predictions from anatomical studies in animals, thus strongly suggesting that fMRI is sufficiently sensitive to discriminate between amygdalar subregions.

Second, although the use of resting-state fMRI data precludes conclusions about specific ongoing cognitive processes in subjects at rest, our results provide proof that this approach has significant utility in understanding network-level abnormalities in psychiatric disorders. Although the degree to which resting-state connectivity reflects real-time, ongoing state properties vs longer-standing trait properties remains uncertain, we and others<sup>10</sup> favor the trait interpretation for several very compelling reasons. A number of studies have examined the topography of resting-state networks during different human behavioral states, including performance of tasks,<sup>77-81</sup> sleep,<sup>82,83</sup> and anesthesia,<sup>84</sup> and in other species,<sup>84</sup> and have found that resting-state networks are largely unaltered despite the highly divergent neural and behavioral contexts being assessed or manipulated. In addition, a large number of simultaneously operating resting-state networks have been identified, and it is unlikely that ongoing mental activity could account for moment to moment fluctuations across so many different brain networks. As a result, it is likely that resting-state networks reflect intrinsic activity possibly related to

synaptic maintenance in critical networks or priming of these networks to allow for rapid activation rather than transient task-related variations in activity.<sup>10</sup> Therefore, group differences in resting-state connectivity most likely reflect group differences in brain structure and connectivity that importantly relate to symptoms, present whether or not the individual is at rest. Moreover, the groups did not differ in connectivity within a control primary auditory network, demonstrating that the group difference in amygdalar connectivity is not due to a global alteration of resting-state connectivity in patients.

Finally, given the correlational nature of fMRI, 1 possible explanation for the connectivity data is that they reflect the confounding effects of physiological variation not related to neural connectivity, arising from cardiac, respiratory, or vascular sources. There are several reasons, however, why these are unlikely to account for our findings. First, we directly accounted for the effects of global signal variation in our regression models and eliminated high-frequency sources of noise by restricting the resting fluctuation frequency band analyzed. In addition, the differentiation between BLA and CMA connectivity was heavily motivated by a large body of anatomical connectivity studies in experimental animals, the results of which were consistent with our functional connectivity findings that we replicated in 2 cohorts of healthy subjects. Moreover, we note that the highly divergent patterns of differential BLA-CMA connectivity arose from source ROIs that abut each other within the small structure of the amygdala. Ours was a study of differential connectivity, comparing the BLA with the CMA, and thus any common effects should be subtracted out in this comparison.

**Submitted for Publication:** December 5, 2008; final revision received February 11, 2009; accepted March 17, 2009.

**Correspondence:** Amit Etkin, MD, PhD, Department of Psychiatry and Behavioral Sciences, Stanford University School of Medicine, 401 Quarry Rd, Stanford, CA 94305 (amitetkin@stanford.edu).

**Author Contributions:** Dr Etkin had full access to all of the data in the study and takes responsibility for the integrity of the data and the accuracy of the data analysis.

**Financial Disclosure:** None reported.

**Funding/Support:** This study was supported by funds for a residency-research program of the Veterans Affairs–Palo Alto Health Care System (Dr Etkin) and grants NS048302 (Dr Greicius), HD047520 (Dr Menon), and NS058899 (Dr Menon) from the National Institutes of Health.

**Additional Contributions:** Eric Kandel, MD, provided helpful comments on the manuscript, and Jennifer Keller, PhD, assisted with planning of the study.

## REFERENCES

- Kessler RC, Keller MB, Wittchen HU. The epidemiology of generalized anxiety disorder. *Psychiatr Clin North Am*. 2001;24(1):19-39.
- Wittchen HU, Hoyer J. Generalized anxiety disorder: nature and course. *J Clin Psychiatry*. 2001;62(suppl 11):15-21.
- Keller MB. The long-term clinical course of generalized anxiety disorder. *J Clin Psychiatry*. 2002;63(suppl 8):11-16.
- Hoffman DL, Dukes EM, Wittchen HU. Human and economic burden of generalized anxiety disorder. *Depress Anxiety*. 2008;25(1):72-90.
- Etkin A, Wager TD. Functional neuroimaging of anxiety: a meta-analysis of emotional processing in PTSD, social anxiety disorder, and specific phobia. *Am J Psychiatry*. 2007;164(10):1476-1488.
- Blair K, Shaywitz J, Smith BW, Rhodes R, Geraci M, Jones M, McCaffrey D, Vythilingam M, Finger E, Mondillo K, Jacobs M, Charney DS, Blair RJ, Drevets WC, Pine DS. Response to emotional expressions in generalized social phobia and generalized anxiety disorder: evidence for separate disorders. *Am J Psychiatry*. 2008;165(9):1193-1202.
- Whalen PJ, Johnstone T, Somerville LH, Nitschke JB, Polis S, Alexander AL, Davidson RJ, Kalin NH. A functional magnetic resonance imaging predictor of treatment response to venlafaxine in generalized anxiety disorder. *Biol Psychiatry*. 2008;63(9):858-863.
- McClure EB, Monk CS, Nelson EE, Parrish JM, Adler A, Blair RJ, Fromm S, Charney DS, Leibenluft E, Ernst M, Pine DS. Abnormal attention modulation of fear circuit function in pediatric generalized anxiety disorder. *Arch Gen Psychiatry*. 2007;64(1):97-106.
- Monk CS, Telzer EH, Mogg K, Bradley BP, Mai X, Louro HM, Chen G, McClure-Tone EB, Ernst M, Pine DS. Amygdala and ventrolateral prefrontal cortex activation to masked angry faces in children and adolescents with generalized anxiety disorder. *Arch Gen Psychiatry*. 2008;65(5):568-576.
- Fox MD, Raichle ME. Spontaneous fluctuations in brain activity observed with functional magnetic resonance imaging. *Nat Rev Neurosci*. 2007;8(9):700-711.
- Greicius MD, Flores BH, Menon V, Glover GH, Solvason HB, Kenna H, Reiss AL, Schatzberg AF. Resting-state functional connectivity in major depression: abnormally increased contributions from subgenual cingulate cortex and thalamus. *Biol Psychiatry*. 2007;62(5):429-437.
- Amaral DG, Price JL, Pitkanen A, Carmichael ST. Anatomical organization of the primate amygdaloid complex. In: Aggleton JP, ed. *The Amygdala: Neurobiological Aspects of Emotion, Memory and Mental Dysfunction*. New York, NY: Wiley-Liss; 1992:1-66.
- Davis M, Whalen PJ. The amygdala: vigilance and emotion. *Mol Psychiatry*. 2001;6(1):13-34.
- LeDoux JE. Emotion circuits in the brain. *Annu Rev Neurosci*. 2000;23:155-184.
- Pitkanen A. Connectivity of the rat amygdaloid complex. In: Aggleton JP, ed. *The Amygdala: A Functional Analysis*. New York, NY: Oxford University Press; 2000:31-115.
- Price JL, Fokje TR, Amaral DG. The limbic region, II: the amygdaloid complex. In: Bjorklund A, Hokfelt T, Swanson LW, eds. *Handbook of Chemical Neuroanatomy*. Vol 5. New York, NY: Elsevier Science Inc; 1987:279-388.
- Heimer L, de Olmos JS, Alheid GF, Pearson J, Sakamoto N, Shinoda K, Marksteiner J, Switzer R. The human basal forebrain, II. In: Bloom FE, Bjorklund A, Hokfelt T, eds. *Handbook of Chemical Neuroanatomy: The Primate Nervous System, Part III*. Vol 15. New York, NY: Elsevier Science Inc; 1999:57-226.
- Eickhoff SB, Heim S, Zilles K, Amunts K. Testing anatomically specified hypotheses in functional imaging using cytoarchitectonic maps. *Neuroimage*. 2006;32(2):570-582.
- Eickhoff SB, Stephan KE, Mohlberg H, Grefkes C, Fink GR, Amunts K, Zilles K. A new SPM toolbox for combining probabilistic cytoarchitectonic maps and functional imaging data. *Neuroimage*. 2005;25(4):1325-1335.
- American Psychiatric Association. *Diagnostic and Statistical Manual of Mental Disorders*. 4th ed. Washington, DC: American Psychiatric Association; 1994.
- Sheehan DV, Lecrubier Y, Sheehan KH, Amorim P, Janavs J, Weiller E, Hergueta T, Baker R, Dunbar GC. The Mini-International Neuropsychiatric Interview (M.I.N.I.): the development and validation of a structured diagnostic psychiatric interview for DSM-IV and ICD-10. *J Clin Psychiatry*. 1998;59(suppl 20):22-33, quiz 34-57.
- Sheehan DV, Lecrubier Y, Harnett-Sheehan K, Janavs J, Weiller E, Bonara LI, Keskiner A, Schinka J, Sheehan MF, Dunbar GC. Reliability and validity of the MINI International Neuropsychiatric Interview (MINI): according to the SCID-P. *Eur Psychiatry*. 1997;12:232-241.
- Spielberger CD, Gorsuch RL, Lushene RE. *Manual for the State-Trait Anxiety Inventory*. Palo Alto, CA: Consulting Psychologists Press; 1970.
- Meyer TJ, Miller ML, Metzger RL, Borkovec TD. Development and validation of the Penn State Worry Questionnaire. *Behav Res Ther*. 1990;28(6):487-495.
- Beck AT, Steer RA. *Beck Anxiety Inventory Manual*. San Antonio, TX: Psychological Corp; 1993.
- Beck AT, Steer RA, Brown GK. *Manual for Beck Depression Inventory II (BDI-II)*. San Antonio, TX: Psychological Corp; 1996.
- Watson D, Clark LA, Weber K, Assenheimer JS, Strauss ME, McCormick RA. Testing a tripartite model. II: exploring the symptom structure of anxiety and depression in student, adult, and patient samples. *J Abnorm Psychol*. 1995;104(1):15-25.
- Watson D, Weber K, Assenheimer JS, Clark LA, Strauss ME, McCormick RA. Testing a tripartite model. I: evaluating the convergent and discriminant validity of anxiety and depression symptom scales. *J Abnorm Psychol*. 1995;104(1):3-14.
- Sridharan D, Levitin DJ, Menon V. A critical role for the right fronto-insular cortex in switching between central-executive and default-mode networks. *Proc Natl Acad Sci U S A*. 2008;105(34):12569-12574.

30. Glover GH, Lai S. Self-navigated spiral fMRI: interleaved versus single-shot. *Magn Reson Med*. 1998;39(3):361-368.
31. Kim DH, Adalsteinsson E, Glover GH, Spielman DM. Regularized higher-order in vivo shimming. *Magn Reson Med*. 2002;48(4):715-722.
32. Friston KJ, Ashburner J, Poline JB, Frith CD, Heather JD, Frackowiak RS. Spatial registration and normalization of images. *Hum Brain Mapp*. 1995;3(3):165-189.
33. Cordes D, Haughton VM, Arfanakis K, Carew JD, Turski PA, Moritz CH, Quigley MA, Meyerand ME. Frequencies contributing to functional connectivity in the cerebral cortex in "resting-state" data. *AJNR Am J Neuroradiol*. 2001;22(7):1326-1333.
34. Amunts K, Kedo O, Kindler M, Pieperhoff P, Mohlberg H, Shah NJ, Habel U, Schneider F, Zilles K. Cytoarchitectonic mapping of the human amygdala, hippocampal region and entorhinal cortex: intersubject variability and probability maps. *Anat Embryol (Berl)*. 2005;210(5-6):343-352.
35. Friston KJ, Holmes AP, Worsley KJ, Poline JB, Frith CD, Frackowiak RS. Statistical parametric maps in functional imaging: a general linear approach. *Hum Brain Mapp*. 1995;2(4):189-210.
36. Eckert MA, Kamdar NV, Chang CE, Beckmann CF, Greicius MD, Menon V. A cross-modal system linking primary auditory and visual cortices: evidence from intrinsic fMRI connectivity analysis. *Hum Brain Mapp*. 2008;29(7):848-857.
37. Murphy K, Birn RM, Handwerker DA, Jones TB, Bandettini PA. The impact of global signal regression on resting state correlations: are anti-correlated networks introduced? *Neuroimage*. 2009;44(3):893-905.
38. Mai JK, Assheuer J, Paxinos G. *Atlas of the Human Brain*. New York, NY: Thieme-Stratton Inc; 1997.
39. Ashburner J, Friston KJ. Unified segmentation. *Neuroimage*. 2005;26(3):839-851.
40. Ashburner J, Friston KJ. Voxel-based morphometry: the methods. *Neuroimage*. 2000;11(6, pt 1):805-821.
41. Nichols T, Brett M, Andersson J, Wager T, Poline JB. Valid conjunction inference with the minimum statistic. *Neuroimage*. 2005;25(3):653-660.
42. Carmichael ST, Price JL. Limbic connections of the orbital and medial prefrontal cortex in macaque monkeys. *J Comp Neurol*. 1995;363(4):615-641.
43. Stefanacci L, Amaral DG. Some observations on cortical inputs to the macaque monkey amygdala: an anterograde tracing study. *J Comp Neurol*. 2002;451(4):301-323.
44. Avendaño C, Price JL, Amaral DG. Evidence for an amygdaloid projection to pre-motor cortex but not to motor cortex in the monkey. *Brain Res*. 1983;264(1):111-117.
45. Shi CJ, Cassell MD. Cascade projections from somatosensory cortex to the rat basolateral amygdala via the parietal insular cortex. *J Comp Neurol*. 1998;399(4):469-491.
46. Sripanidkulchai K, Sripanidkulchai B, Wyss JM. The cortical projection of the basolateral amygdaloid nucleus in the rat: a retrograde fluorescent dye study. *J Comp Neurol*. 1984;229(3):419-431.
47. Amaral DG, Price JL. Amygdalo-cortical projections in the monkey (*Macaca fascicularis*). *J Comp Neurol*. 1984;230(4):465-496.
48. Ghashghaei HT, Hilgetag CC, Barbas H. Sequence of information processing for emotions based on the anatomic dialogue between prefrontal cortex and amygdala. *Neuroimage*. 2007;34(3):905-923.
49. Ochsner KN, Gross JJ. The cognitive control of emotion. *Trends Cogn Sci*. 2005;9(5):242-249.
50. Johnstone T, van Reekum CM, Urry HL, Kalin NH, Davidson RJ. Failure to regulate: counterproductive recruitment of top-down prefrontal-subcortical circuitry in major depression. *J Neurosci*. 2007;27(33):8877-8884.
51. Urry HL, van Reekum CM, Johnstone T, Kalin NH, Thurov ME, Schaefer HS, Jackson CA, Frye CJ, Greischar LL, Alexander AL, Davidson RJ. Amygdala and ventromedial prefrontal cortex are inversely coupled during regulation of negative affect and predict the diurnal pattern of cortisol secretion among older adults. *J Neurosci*. 2006;26(16):4415-4425.
52. Wager TD, Davidson ML, Hughes BL, Lindquist MA, Ochsner KN. Prefrontal-subcortical pathways mediating successful emotion regulation. *Neuron*. 2008;59(6):1037-1050.
53. Price JL, Amaral DG. An autoradiographic study of the projections of the central nucleus of the monkey amygdala. *J Neurosci*. 1981;1(11):1242-1259.
54. Reardon F, Mitrofanis J. Organisation of the amygdalo-thalamic pathways in rats. *Anat Embryol (Berl)*. 2000;201(1):75-84.
55. Holschneider DP, Yang J, Sadler TR, Nguyen PT, Givrad TK, Maarek JM. Mapping cerebral blood flow changes during auditory-cued conditioned fear in the nontethered, unrestrained rat. *Neuroimage*. 2006;29(4):1344-1358.
56. Yasoshima Y, Scott TR, Yamamoto T. Differential activation of anterior and midline thalamic nuclei following retrieval of aversively motivated learning tasks. *Neuroscience*. 2007;146(3):922-930.
57. Van der Werf YD, Witter MP, Groenewegen HJ. The intralaminar and midline nuclei of the thalamus: anatomical and functional evidence for participation in processes of arousal and awareness. *Brain Res Brain Res Rev*. 2002;39(2-3):107-140.
58. Supple WF Jr, Leaton RN, Fanselow MS. Effects of cerebellar vermal lesions on species-specific fear responses, neophobia, and taste-aversion learning in rats. *Physiol Behav*. 1987;39(5):579-586.
59. Sacchetti B, Baldi E, Lorenzini CA, Bucherelli C. Cerebellar role in fear-conditioning consolidation. *Proc Natl Acad Sci U S A*. 2002;99(12):8406-8411.
60. Sacchetti B, Sacco T, Strata P. Reversible inactivation of amygdala and cerebellum but not perirhinal cortex impairs reactivated fear memories. *Eur J Neurosci*. 2007;25(9):2875-2884.
61. Heath RG, Dempsey CW, Fontana CJ, Myers WA. Cerebellar stimulation: effects on septal region, hippocampus, and amygdala of cats and rats. *Biol Psychiatry*. 1978;13(5):501-529.
62. Snider RS, Maiti A. Cerebellar contributions to the Papez circuit. *J Neurosci Res*. 1976;2(2):133-146.
63. Schmahmann JD, Sherman JC. The cerebellar cognitive affective syndrome. *Brain*. 1998;121(pt 4):561-579.
64. Seeley WW, Menon V, Schatzberg AF, Keller J, Glover GH, Kenna H, Reiss AL, Greicius MD. Dissociable intrinsic connectivity networks for salience processing and executive control. *J Neurosci*. 2007;27(9):2349-2356.
65. Critchley HD. Neural mechanisms of autonomic, affective, and cognitive integration. *J Comp Neurol*. 2005;493(1):154-166.
66. Hoehn-Saric R, McLeod DR, Funderburk F, Kowalski P. Somatic symptoms and physiologic responses in generalized anxiety disorder and panic disorder: an ambulatory monitor study. *Arch Gen Psychiatry*. 2004;61(9):913-921.
67. Thayer JF, Friedman BH, Borkovec TD. Autonomic characteristics of generalized anxiety disorder and worry. *Biol Psychiatry*. 1996;39(4):255-266.
68. Duncan J, Owen AM. Common regions of the human frontal lobe recruited by diverse cognitive demands. *Trends Neurosci*. 2000;23(10):475-483.
69. Miller EK, Cohen JD. An integrative theory of prefrontal cortex function. *Annu Rev Neurosci*. 2001;24:167-202.
70. Aikins DE, Craske MG. Cognitive theories of generalized anxiety disorder. *Psychiatr Clin North Am*. 2001;24(1):57-74, vi.
71. Wells A. A cognitive model of generalized anxiety disorder. *Behav Modif*. 1999;23(4):526-555.
72. Mathew SJ, Mao X, Coplan JD, Smith EL, Sackeim HA, Gorman JM, Shungu DC. Dorsolateral prefrontal cortical pathology in generalized anxiety disorder: a proton magnetic resonance spectroscopic imaging study. *Am J Psychiatry*. 2004;161(6):1119-1121.
73. Bystritsky A, Kaplan JT, Feusner JD, Kerwin LE, Wadekar M, Burock M, Wu AD, Iacoboni M. A preliminary study of fMRI-guided rTMS in the treatment of generalized anxiety disorder. *J Clin Psychiatry*. 2008;69(7):1092-1098.
74. Etkin A, Klemenhagen KC, Dudman JT, Rogan MT, Hen R, Kandel ER, Hirsch J. Individual differences in trait anxiety predict the response of the basolateral amygdala to unconsciously processed fearful faces. *Neuron*. 2004;44(6):1043-1055.
75. Morris JS, Buchel C, Dolan RJ. Parallel neural responses in amygdala subregions and sensory cortex during implicit fear conditioning. *Neuroimage*. 2001;13(6, pt 1):1044-1052.
76. Whalen PJ, Shin LM, McInerney SC, Fischer H, Wright CI, Rauch SL. A functional MRI study of human amygdala responses to facial expressions of fear versus anger. *Emotion*. 2001;1(1):70-83.
77. Arfanakis K, Cordes D, Haughton VM, Moritz CH, Quigley MA, Meyerand ME. Combining independent component analysis and correlation analysis to probe interregional connectivity in fMRI task activation datasets. *Magn Reson Imaging*. 2000;18(8):921-930.
78. Fox MD, Corbetta M, Snyder AZ, Vincent JL, Raichle ME. Spontaneous neuronal activity distinguishes human dorsal and ventral attention systems. *Proc Natl Acad Sci U S A*. 2006;103(26):10046-10051.
79. Fox MD, Snyder AZ, Vincent JL, Corbetta M, Van Essen DC, Raichle ME. The human brain is intrinsically organized into dynamic, anticorrelated functional networks. *Proc Natl Acad Sci U S A*. 2005;102(27):9673-9678.
80. Fransson P. How default is the default mode of brain function? further evidence from intrinsic BOLD signal fluctuations. *Neuropsychologia*. 2006;44(14):2836-2845.
81. Greicius MD, Menon V. Default-mode activity during a passive sensory task: uncoupled from deactivation but impacting activation. *J Cogn Neurosci*. 2004;16(9):1484-1492.
82. Fukunaga M, Horovitz SG, van Gelderen P, de Zwart JA, Jansma JM, Ikonomidou VN, Chu R, Deckers RH, Leopold DA, Duyn JH. Large-amplitude, spatially correlated fluctuations in BOLD fMRI signals during extended rest and early sleep stages. *Magn Reson Imaging*. 2006;24(8):979-992.
83. Horovitz SG, Fukunaga M, de Zwart JA, van Gelderen P, Fulton SC, Balkin TJ, Duyn JH. Low frequency BOLD fluctuations during resting wakefulness and light sleep: a simultaneous EEG-fMRI study. *Hum Brain Mapp*. 2008;29(6):671-682.
84. Vincent JL, Patel GH, Fox MD, Snyder AZ, Baker JT, Van Essen DC, Zempel JM, Snyder LH, Corbetta M, Raichle ME. Intrinsic functional architecture in the anaesthetized monkey brain. *Nature*. 2007;447(7140):83-86.